國 立 成 功 大 學
醫 學 工 程 研 究 所
碩 士 論 文

Coil Design of Repetitive Transcranial Magnetic Stimulation System for Small Animal

設計重複性顱磁刺激治療系統之線圈應用於動物實驗

研究生:陳怡誠
指導教授:陳家進

中華民國九十七年七月

國立成功大學

碩士論文

設計重複性顱磁刺激治療系統之線圈應用於動物實驗

Coil Design of Transcranial Magnetic Stimulation System for Small Animal

研究生：陳怡誠

本論文業經審查及口試合格特此證明

論文考試委員：

指導教授：

系(所)主管：

中 華 民 國 97 年 7 月 11 日

國立成功大學

碩士論文

設計重複性顱磁刺激治療系統之線圈應用於動物實驗

Coil Design of Transcranial Magnetic Stimulation System for Small Animal

研究生：陳怡誠

本論文業經審查及口試合格特此證明

論文考試委員：

指導教授：

系(所)主管：

中 華 民 國 97 年 7 月 11 日

中文摘要

重複性顱磁刺激(repetitive transcranial magnetic stimulation)就是一項非侵入式利用電生磁、磁生電去刺激腦部、神經與肌肉等特定部位的技術，提供潛在的好處對於各種神經病學與精神病學的疾病進行治療。儘管有許多的研究及治療方式陸續發展，但目前仍缺乏線圈磁場聚焦性與強度改善的相關研究，因此，如何有效控制電磁場強度與聚焦性提高一直是重複性顱磁刺激最重要的問題。

本研究的目的在設計微小線圈應用在動物實驗上，首先，在線圈中心加入鐵核來改善磁場穿透能力大小，使用水冷卻循環系統來達到冷卻目的。再來，設計不同銅屏蔽的大小與開孔位置，並透過磁場量測平台測試磁場分佈，比較各種屏蔽設計的優缺點，達到改善聚焦性能。將此設計應用於動物實驗上，探討運動誘發電位(motor evoked potential)在沒有遮蔽的線圈與加上不同屏蔽的線圈是否能準確性的誘發，發現加上屏蔽的線圈雖然改善聚焦能力但必須要有足夠的磁通量才能誘發感應電勢。另外加上屏蔽的線圈會產生聲響而造成聽覺驚嚇反射（auditory startle reflex ）動作誘發出 MEP，因此利用分貝計來判斷，在多少分貝以上才會造成。

關鍵詞: 重複顱磁刺激、線圈設計、屏蔽、運動誘發電位

Abstract

Repetitive transcranial magnetic stimulation (rTMS) is a non-invasive technique to stimulate the brain, nerve and muscle by electric fields that are generated from an excitation coil. rTMS offers potential benefit as a therapeutic treatment for a variety of neurological and psychiatric disorders. Although various rTMS schemes have been developed for clinical studies, there is a lack of the coil for generating localized magnetic field with enhanced intensity for rTMS in small animal. The aim of this study was to design a miniature stimulation coil for rTMS studies in small animal. First, a circular coil with iron-core for improving the penetration of the magnetic field was designed which was equipped with a water cooling apparatus to prevent from over heat. In addition, the shields of varied sizes and shapes were employed to localize the stimulation area which distribution was measured in a magnetic field recording platform using Hall effect probe controlled by 2D step motor. Our results indicated that copper plate of 1 mm thickness with proper opening can shield well and provide localized stimulation to elicit motor evoked potential (MEP). However, the shock wave generated by magnetic stimulation was enhanced during the shielding experiment which might elicit auditory startle reflex (ASR) instead of MEP. Thus, a better sound proof design to reduce the sound below 96 dB should be taken into consideration when design a shielded rTMS for small animal.

Keywords: repetitive transcranial magnetic stimulation, coil design, shielding, motor evoked potential

誌　謝

三年的研究生涯繞了一大圈終於告一段落。在此特別感謝指導教授陳家進老師，不僅在研究上的悉心指導，也讓我去追尋自己的職業生涯，雖然曾經一度想放棄研究，但老師仍不斷勉勵與支持，替我解決研究上的瓶頸，讓我勇敢堅持下去，衷心感謝您不辭辛勞的為我付出。也感謝蔡德明老師在電磁研究方面時給予的寶貴建議，以及鄭國順老師與梁治國老師口試上給予的指導和建議，在此謹致最深的敬意。

另外最要感謝是同組的宗勳學長和尚衡學弟，在整個研究的觀念、儀器的架構及動物實驗的部分都給予我許多的幫助與支持，沒有學長您指導本論文是無法順利完成，而在日常生活上也給我極大的鼓勵。也感謝當初與我一起打拼伙伴家禾、治宏、力夫、建儀、恩廷、階曉、守來們在研究與課業上相互學習與討論，並帶給我生活上許多的建議及歡樂，還有珍貴的友誼。此外，還要感謝彰師附工阿強、朝洋、弘明、俞婷、忠樸、智泓、旺泉、建鋒、宜弘和員林農工雅晶的打氣與幫忙，讓我有更充裕時間準備使研究路程上更加平順與安穩。

還有我最親愛的爸爸與媽媽，哥哥、妹妹和舅舅的支持、照顧與關心，因為你們的鼓勵讓我決定繼續唸碩士，在我最失落的時候，你們是我最大的精神支柱，也因此才有今天的成就，感謝你們這些日子的陪伴及容忍。

最後謹以此論文獻給我深愛的家人及賢師益友，沒有您們就沒有今天的我，感謝您們。

Contents

List of Figures

List of Tables

Chapter 1 Introduction

1.1 Introduction of repetitive transcranial magnetic stimulation

Transcranial magnetic stimulation (TMS) is a non-invasive technique to excite neuronal tissue in vivo by a time-varying, intensity magnetic field generated by a fast electric pulse within a stimulation coil placed close to brain. In recent years, rTMS has been proven to be useful as an alternative to electroshock therapy for the treatment of depression, Parkinson's disease, and others. The principle of TMS is to pass a brief surge of current through a coil of copper wires, which induces a rapidly changing magnetic field. This magnetic field passes into the surrounding medium, where it again induces an electrical field and tends to decrease or increase the function of brain neuronal cells. The schematic diagram of TMS is depicted in Figure 1.1[1].

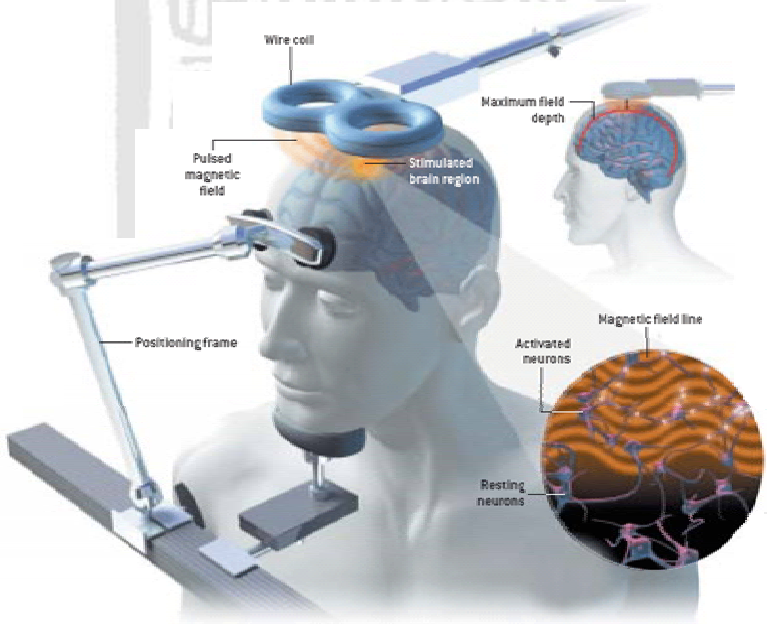

Figure 1.1. The schematic diagram of the transcranial magnetic stimulation [1].

The operation principle of the magnetic stimulation device is illustrated in Figure 1.2. In this schematic diagram, C is capacitor for charging and discharging, L is the magnetic coil, R is the resistance coil, and U is power supply with two switches. The circuit consists of two main loops that the charging loop (I_C) and the discharging loop

(I_L). During the charging phase, switch 1 is closed and switch 2 is open. The capacitor is charged to the peak DC voltage provided by the power supply. Entering the discharging phase, the switch 1 is then opened and switch 2 is closed. The capacitor discharges current quickly through the excitation coil and yields the rate of change of the magnetic field, thus causing higher induced electrical fields. The source of activation is the electric field induced in the tissue, obtained from Faraday's law

$$\nabla \times \vec{E} = -\frac{\partial \vec{B}}{\partial t}$$

where B is the magnetic field produced by the coil, given by the Biot-Savart law:

$$\vec{B}(r,t) = \frac{\mu_0}{4\pi} I(t) \oint_c \frac{\vec{dI} \times \vec{R}}{R^2}$$

The two switches are controlled by multivibrator and timing pulse circuit [2].

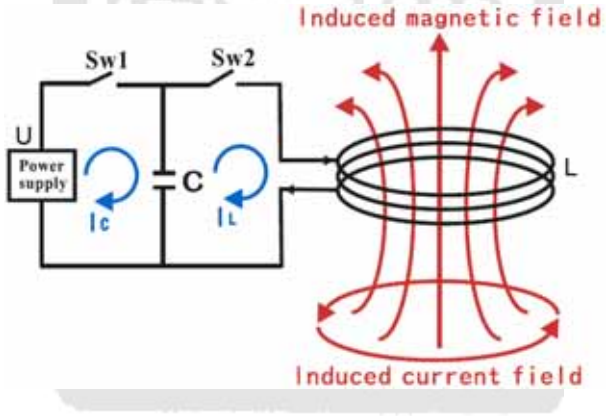

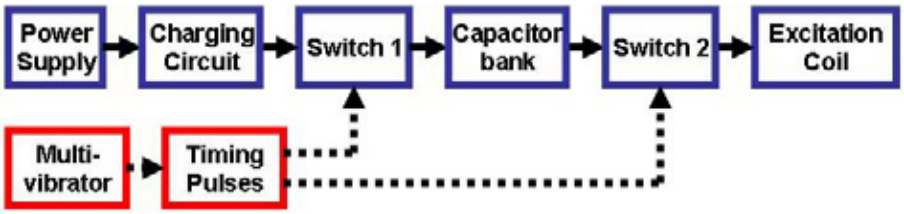

Figure 1.2 The schematic diagram of control circuit for TMS.

TMS of single magnetic pulse can only produce the immediate effects. For example, when researchers send a single magnetic pulse into the motor cortex of a subject's brain, it produces a jerk in the hand, arm, face or leg, depending on where

the coil is placed. In contrast, repetitive TMS (rTMS) is a series of magnetic pulses of continuous cycles which cause physiological responses differing from single pulse TMS. Repetitive TMS can inhibit or facilitate the brain functions. In general, the stimulation of frequency above 5 Hz is called high-frequency rTMS and that below 1 Hz is called low-frequency rTMS. This distinction is important because these two types of stimulation have opposite effects on brain physiology. Several initial studies of high-frequency rTMS to increase cortical excitability and of low-frequency rTMS to decrease cortical excitability have shown improvement in depressive symptoms [3].

1.2 Influencing factors of magnetic stimulation

In commercially available magnetic stimulation coil, most of them are employed for human. From the following equations, we can find that several factors may affect the magnetic stimulation including coil configuration, coil size and number of turns per loop [4].

From Maxwell equation's Faraday law

$$\nabla \times \vec{E} = -\frac{\partial \vec{B}}{\partial t} \tag{1}$$

From (1) it also can be written

$$\iint_S \left(\nabla \times \vec{E}\right) \cdot d\vec{S} = \iint_S \left(-\frac{\partial \vec{B}}{\partial t}\right) \cdot d\vec{S} \tag{2}$$

From Stokes's theorem

$$\iint_S \left(\nabla \times \vec{E}\right) \cdot d\vec{S} = \oint_C \vec{E} \cdot d\vec{l} \tag{3}$$

And (3) can be written

$$\oint_C \vec{E} \cdot d\vec{l} = \iint_S \left(-\frac{\partial \vec{B}}{\partial t}\right) \cdot d\vec{S} \tag{4}$$

Finally,

$V_{in} = -\frac{d\Phi}{dt} = -N\frac{d(BA)}{dt}$, where $V_{in} = \oint_c \vec{E} \cdot d\vec{l}$ and $\Phi = \iint_s \vec{B} \cdot d\vec{S}$ (5)

We can obtain $\frac{dB}{dt} = \frac{V_{in}}{NA}$,

For the coil configuration, the excitation area and ratio between the primary and secondary peaks of magnetic stimulation increase with slinky loop number. The direction of the induced electric field tends to be more parallel and aligned in one direction with increasing number of loops. The butterfly coil has been shown to have higher spatial resolution than the circular coil. Secondly, the size of coil determines the excitation area and the secondary peaks which increase with the increase of coil diameter. As an increase in the coil diameter, decrease in the ratio between the primary and secondary peaks can be found. Finally, the electric field increases with less turns per loop [4].

1.3 Various types of coil designs

Various types of magnetic coils including circular coil, butterfly coil, and three dimensional coils etc, have been designed [4, 5]. The circular coils and butterfly coils have been commonly used in clinical studies. It is important to note that the current induced by circular coil is near zero on the central axis of the coil and increases to a maximum in a ring under the mean diameter of the coil. Stimulation occurs under the winding and not under the coil centre. The butterfly coil induces the maximum current directly under its center, where the two windings meet, giving a more accurately defined area of stimulation. However, both types of coils are in poor localization and hence lack of precision in stimulating the specific structures in the brain [6, 7, 8]. To improve field localization of magnetic stimulation, several coil designs such as slinky coil, three dimensional differential coil, iron-core coil, multi-channel coil and shield

plate have been proposed [5, 9, 10 , 11].

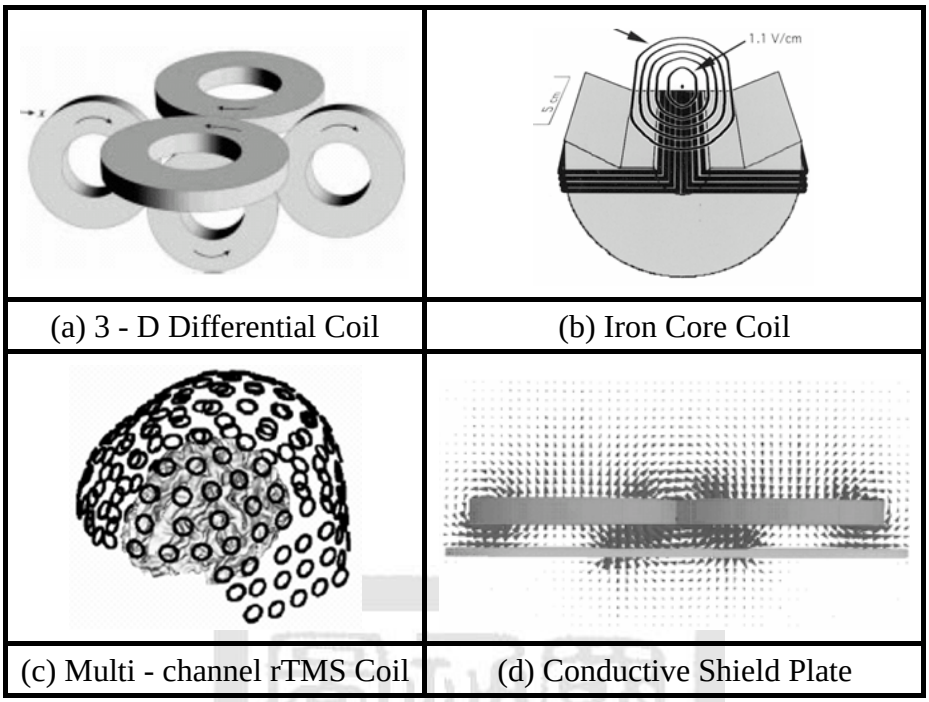

(a) 3 - D Differential Coil | (b) Iron Core Coil

(c) Multi - channel rTMS Coil | (d) Conductive Shield Plate

Figure 1.3. Various designs of magnetic stimulation coils.

The slinky coil is formed by winding different numbers of loops forming a helical coil on a half torus. Although the extra loops of a slinky coil can enhance the induced field, the localization becomes worse than the figure-of-eight (FOE) coil [4]. Three dimensional differential coil design consists of a butterfly coil with two additional wing units and an extra bottom unit, as shown in Figure 1.3(a). The wing units produce opposite fields to restrict the spread of induced fields. The bottom unit further enhances the induced fields at the excitation site. Although the device can improve field localization, the efficiency using this design is lower than the FOE coil [5]. Iron-core TMS coil consists of the FOE coil fits into the center and side spaces of the core, as shown in Figure 1.3(b). Using ferromagnetic cores in coil can reduce power requirements and heat generation which can further improve the penetration of the magnetic field [9, 12]. A specific multi-channel coil consists of 119 coils in which each coil is an independent driving circuit for independent control, as shown in Figure

1.3(c). The device can be conveniently used for precise deep brain stimulation and simultaneous stimulation of multiple locations. With the increased number of stimulation coils, the intensity of magnetic field at the same location increased and the stimulation depth was significantly improved [10, 13, 14].

In order to improve field localization, an effective and practical solution is to utilize conductive shield plate inserted between the stimulation coil and the brain, as shown in Figure 1.3(d). The shield can improve the induced field localization by more than 50% and prevent other parts of the brain from exposure to high pulsed magnetic fields [11]. Summary of various magnetic stimulation coils is listed in Table 1.1.

Table. 1.1. Comparison among various designs of magnetic stimulation coils

	Advantages	Disadvantages
Slinky coil	enhance the induced field	lower spatial resolution
3-D differential coil	higher spatial resolution	lower efficiency
Iron-core coil	reduce power requirements reduce heat generation higher penetration ability	saturation of core
Multi-channel coil	higher spatial resolution higher penetration ability simultaneous stimulation of different locations	necessary a great of power not easy to fabricate
Shielding plate	higher spatial resolution	Reduce the induced field

1.4 Motivation and the aims of this study

In recent years, rTMS on the human and rat's brain has been proposed as a therapeutic tool in a variety of psychiatric and neurological disorders [15, 16]. Before TMS can be applied effectively in clinical trial, various rTMS studies should be experimented on small animals. However, the rat's brain is much smaller than human brain, the magnetic coil designed for the human subject is too large for defining

specific brain area of rat. In order to obtain accurate distribution of electric field, several rTMS coils were specially developed for application in small mammals [17]. To design the coil for small animals, several factors including localization of stimulation and strong enough stimulation should be taken into consideration in the design of coil.

The aim of this study was to design a miniature rTMS coil which can be used for localized stimulation of rat's brain. First, one special circular coil with the ferromagnetic iron core was designed for improving the penetration of the magnetic field, reducing power requirements and generating less heat than air-core. In addition, conductive shielding plates of various shapes and openings were utilized to provide highly localized induced fields. The conductive shielding plate can be placed between the custom rTMS coil and the brain from which we can alter the shielding window size and position to improve the stimulation localization and effectiveness. Finally, a custom-designed water cooling system was adopted for elongating the course of treatment [18]. For assessing the distribution of magnetic stimulation, a magnetic field measurement platform for measuring the focality of rTMS coil was designed. The stimulation shield was tested in animal to validate the feasibility of evoking motor potential.

Chapter 2 Materials and Methods

2.1 Overall structure of rTMS for small animal

Figure 2.1 shows the overall structure of rTMS assessment platform for coil and shielding design. The rTMS device unit consists a magnetic stimulator device (Magstim Ltd., Whitland, Dyfed, UK) and FOE coil. The stimulus waveform was biphasic with a maximum peak magnetic field of about 3.5 Tesla, 1 Hz to 100 Hz stimulation frequency achievable (100% output up to 25 Hz, 50% output at 50 Hz, 30% output at 100 Hz) and a pulse width of 400 μs.

The magnetic field measurement platform consists a 2D positioning device (Yamaha, T5P06-50), Guass meter and Hall effect probe (Hirst Magnetic Instruments, LTD.). Figure 2.2 shows the experimental setup of rTMS for animal studies. An amplifier was used to record the MEP of hindlimb for assessing the motor excitability. The recorded MEP was monitored from oscilloscope and sampled by analogue to digital converter for further analysis.

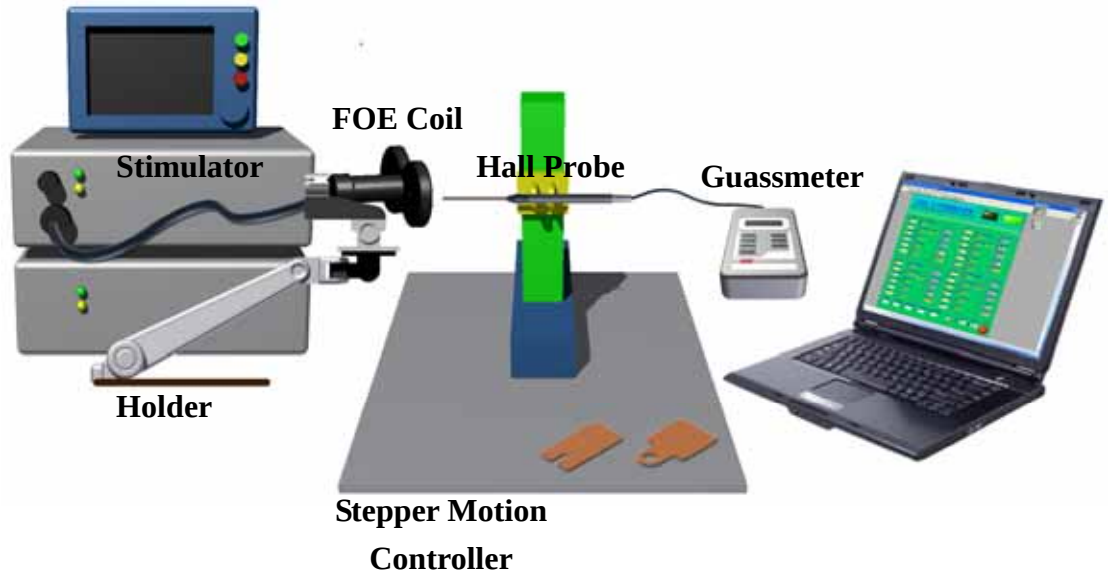

Figure 2.1. Overall structure of rTMS device and magnetic field measurement platform.

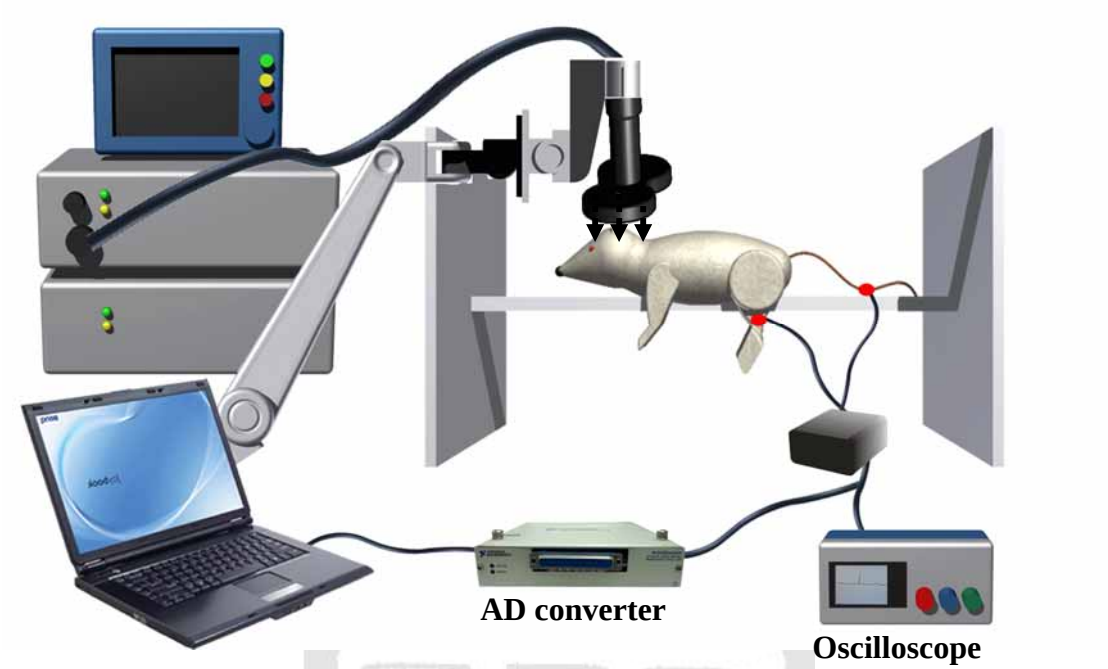

Figure 2.2. Schematic diagram of applying rTMS for rat studies.

2.2 Magnetic field measurement platform

2.2.1 Positioning control unit

In order to measure the magnetic field of the coil in 2D plane, we utilized x-y axes step motor to control the position of measurement probe in x and y axes. The controller (ADLINK, LTD. PCI-8132) can generate high frequency pulses to drive stepping motors (Yamaha, LTD. T5P06-50).

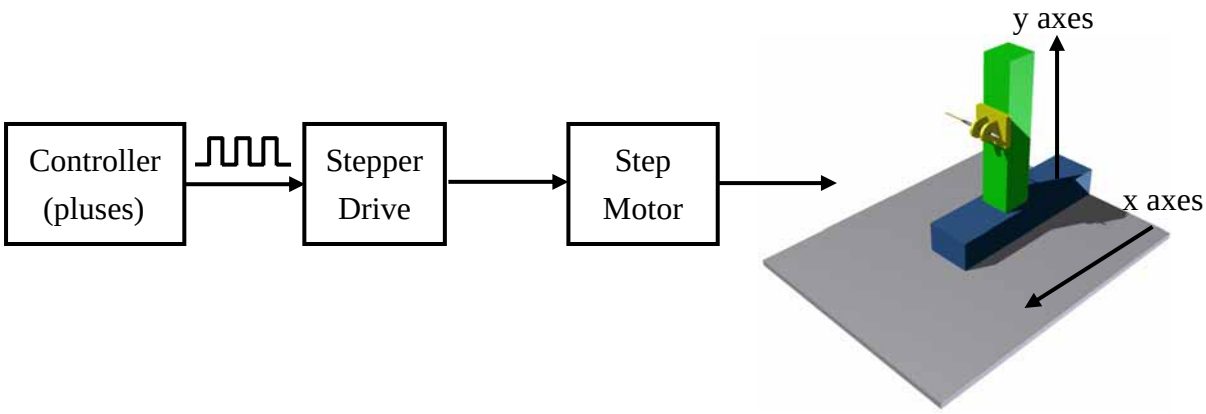

Figure 2.3. Block diagram of step motor.

Table. 2.1. The specifications of the 2D positioning controller

PCI-8132 motion control card Specifications	
Motion	1. Number of controllable axes: 2 2. Max. number of cards in one system: 12 3. 0.03pps to 2.4Mpps programmable DIR/OUT, CW/CCW pulse command output 4. Max. acceleration rate: 91Mpps^2 5. Speed resolution: 16-bit 6. One 28-bit counter for encoder input of each axis 7. Positioning range: -134,217,728 to +134,217,727 (28-bit) 8. Encoder input frequency: 2.4MHz @ 3M cable 9. 16-Ch input & 16-Ch output

A graphical user interface (GUI) written in Labview program, as shown in Figure 2.4 is used to setup the parameters of speed and position for the stepper motor. These parameters include the moving distance and direction and pause time interval for rTMS stimulation and recording.

Figure 2.4. The graphical user interface developed in Labview for selecting the speed and position parameters.

2.2.2 Gauss meter unit

In order to measure the magnetic field generated by stimulation coils, we use gaussmeter GM08 and Hall probe to measure the distribution of magnetic field. The specifications of the gaussmeter are listed in Table 2.1. The operation principle of Hall probe is based on the Hall effect of a small slab of semi-conductor material of Hall element. The current passes from one end of the slab to the other from which the voltage on each end of the slab can be maintained when no magnetic field is present. If a magnetic field is applied through the top to bottom surfaces of the slab, the voltage across the sides of the slab is directly proportional to the magnetic flux density or magnetic field strength as shown in Figure 2.5.

Table. 2.2. The specifications of the gaussmeter

GM08 Specifications	
Model	GM08
Range 1 Range 2 Range 3 Range 4	0.000 - ±3.000 Tesla 000.0 - ±299.9 milliTesla 00.00 - ±29.99 milliTesla 00.00 - ±2.999 milliTesla
Frequency Range	DC and 15 Hz to 10 kHz
Units	Tesla, Gauss, Amps/m or Oersted
Functions	DC (DC magnetic field measurement) DC peak (Maximum positive peak reading of the DC field) AC RMS (True RMS of input signal) AC PEAK (Maximum true RMS) AC MAX (Maximum positive peak reading of the AC field)
Accuracy	Better than ±1% Probe and Gaussmeter
Features	Support USB and RS232

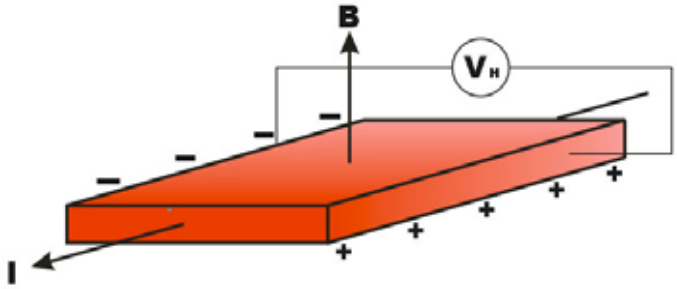

Figure 2.5. The principle of Hall effect for detecting magnetic flux intensity.

Various Hall probes have been designed from which transverse and axial probes were used in this study, as shown in Figure 2.6. The sensing part of the Hall probe is placed in the magnetic field at right angle to the magnetic lines of flux to obtain the maximum reading. Since the step motor used in this study can only move in x-y direction, we need to use axial probe first to record magnetic flux intensity in x-y direction and change the depth of the rTMS coil for that in z direction.

Figure 2.6. The use of (a) axial probe and (b) transverse probe for recording the magnetic flux in different orientations.

2.3 Evaluation of shielding plate

During coil design, it is essential to evaluate the induced magnetic field generated by coil. For our animal study, focused stimulation is needed for small stimulation site in rat's brain. A family of copper plates was designed and constructed

as shown in Figure 2.7. The copper plate with conductivity of $5.8\times10^{7} S/m$ was selected as shielding plate. The thickness of shielding plate should be at least thicker than 1 mm. Various shapes of shielding plates were cut for testing the geometric effect. The corner surfaces of copper plate were filleted to prevent induced electric fields from being locally concentrated on sharp corners.

Various shielding plates were compared with the measurement without shielding. Our experimental shields include a hole in the copper plate, half-sized copper plate, an open area of a quarter of the left side corner, and open at one eighth of the copper plate, and an open rectangular window.

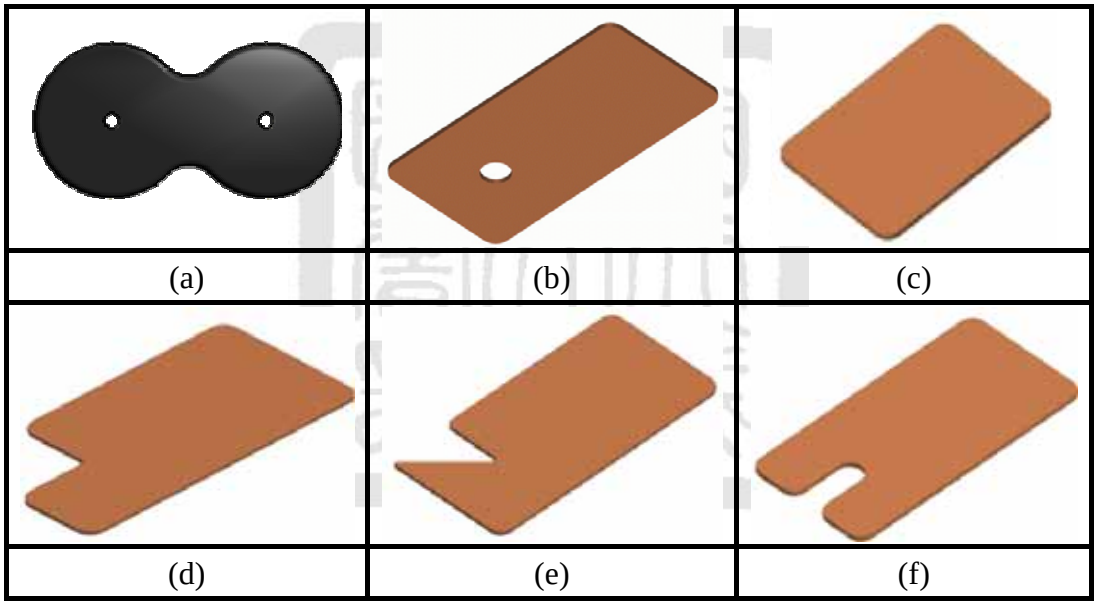

Figure 2.7. Various types of shielding plates include (a) without shield plate, (b) shield plate with a hole, (c) half-sized shield plate, (d) a quarter of the shield plate, (e) one eighth of the shield plate, and (f) open rectangular window of the shield plate.

A custom-made FOE coil with a mean diameter of 50 mm was selected as a reference coil. The X-Y stepper motor was used to control the position of Hall probe. Due to the limitation on the moving range of step motor, the measurement of the left and right circular coils would be performed separately. Each measurement area is 50

mm × 50 mm with 40 × 20 measurement points, in a total of 800 points. The right upper corner is set to be the origin point. $P_1(0,0)$, during the measurement of the right circular coil. Similarly, the left upper corner is set to be the origin point, $P_2(0,0)$, for the left circular coil. The measurements was performed from up to down and right to left, as shown in Figure 2.8.

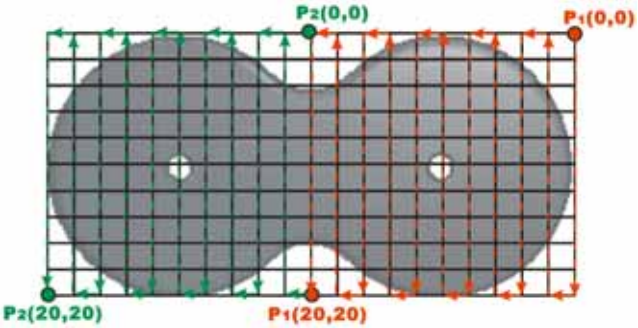

Figure 2.8. The probe measures the trajectory.

The point-to-point measurements of instantaneous magnetic field generated from the rTMS were mapped with respect to the FOE. First experiment was aimed to measure the effect of magnetic flux in perpendicular to various planes of XY, ZX, ZY, as shown in Figure 2.9. The magnetic intensity in XY, ZX, and ZY are denoted the intensity in Fz, Fy, and Fx axes. The axial probe was used to measure XY plane while the transverse probe was applied to measure ZX and ZY planes. The overall magnetic field intensity should be the square root of the sum of the squares of magnetic intensity of each plane ($R = \sqrt{F_x^2 + F_y^2 + F_z^2}$). Experiments were also designed to evaluate the magnetic distributions of various power outputs of TMS at varied distances toward the coil surface. Furthermore, shielding plates shown in Figure 2.7 were tested from which the peak magnitude and the half power region (HPR) were measured to observe the effective stimulation area.

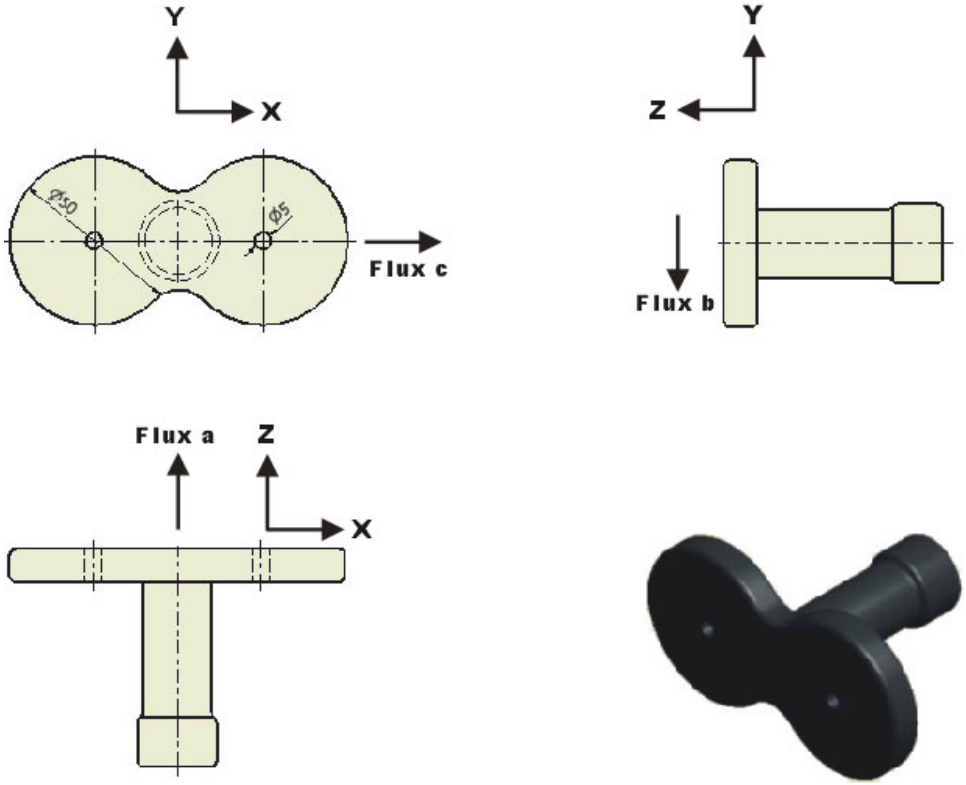

Figure 2.9. The use of Hall probes to measure the magnetic flux in 3 different planes.

2.4 Construction of magnetic stimulation coil

To improve the efficiency of rTMS coil, several coil designs for human and animal have been proposed [19, 20]. A custom-made rTMS coil was specially designed for application in small mammals. The inner and outer radii of the loops of coil are 25 mm and 40 mm, respectively. Each coil consisted of 47 loops of round copper wire (Φ=1 mm^2), as shown in Figure 2.10. It was designed in a slightly concave form for an optimal fitting to the animal's head. The thickness of the plastic chassis is 2 mm on the side attached to the vertex of the rat's head model. However, the coil could produce large amount of heat and cause rise in temperature. A overheat protection has been installed in the rTMS device toe avoid the breakdown of rTMS. To perform longer stimulation period, a cooling system is highly desired. In order to improve overheated problem, we utilized a water cooling system to dissipate the heat

generated during magnetic stimulation.

Figure 2.10. Construction of magnetic stimulation coil.

2.5 Animal experiments

To test the rTMS on animal, animals were anaesthetized with chloral hydrate (400 mg/kg i.p.). TMS was applied to adult male Wistar rats (300 g ~ 400 g body weight) while the animals were anesthetized and fixated in a stereotaxic frame. All four limbs were hanged down and the hindlimb to place electrodes. Figure 2.2 illustrates the stimulation and recording setup for determining transcranial magnetic motor evoked potentials (TMMEPs).

The electromyogram (EMG) was recorded bilaterally from the calf muscles

(gastrocnemius). Resting motor threshold (RMT) was determined every trial before rTMS stimulation. MT was defined as the magnetic stimulus intensity just able to induce a visible twitch in the right hindlimb. To determine resting motor threshold (RMT) in rat, the animal was placed on the plate with its rear legs hanging out. RMT was determined by increasing magnetic stimulation intensity in steps of 4 percentage points of absolute stimulator output starting with intensities that did not produce MEP responses.

RMT was defined as the magnetic stimulus intensity just able to induce a MEP (over 50μV) in the hind limb. The intensity was increased until 10 of 10 suprathreshold MEP were observed. MEP with an amplitude 50 μV was considered suprathreshold. After RMT determination, 10 MEP's were recorded for 120% of MT intensities with an interstimulus interval of 10s. The recruitment curve was also plotted from those measured from the intensity of 80%, 90%, 100%, 110%, 120%, 130%, 140%, 150%, 160% of RMT [21, 22, 23].

Chapter 3 Results

3.1 Factors influencing the magnetic field distribution

Figure 3.1 shows the distribution of magnetic field around the TMS coil without shielding at power level of 50 %. We can observe that peak magnetic flux occurs near the center of coil of FOE which is similar to the specification given by the manufacturer. However, the peak intensity of magnetic field of the left coil is higher than that of right one.

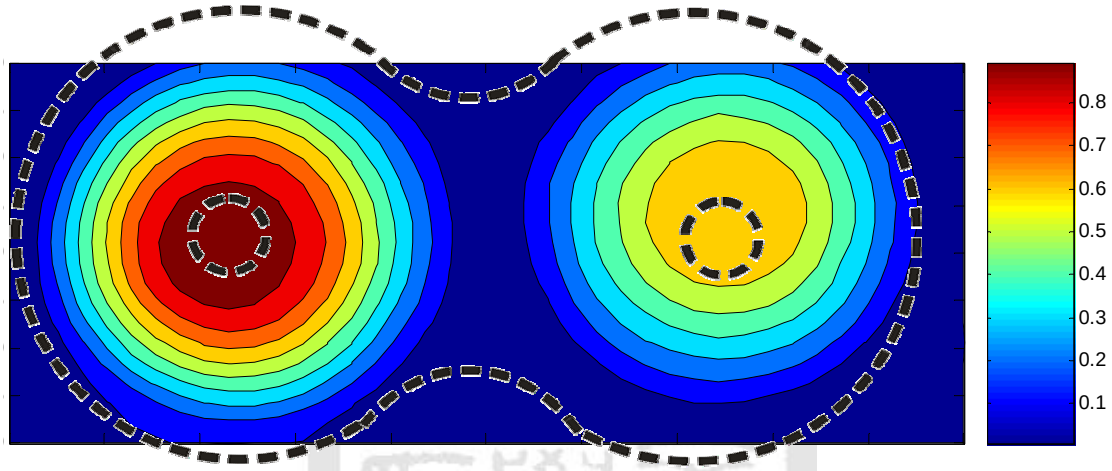

(a)

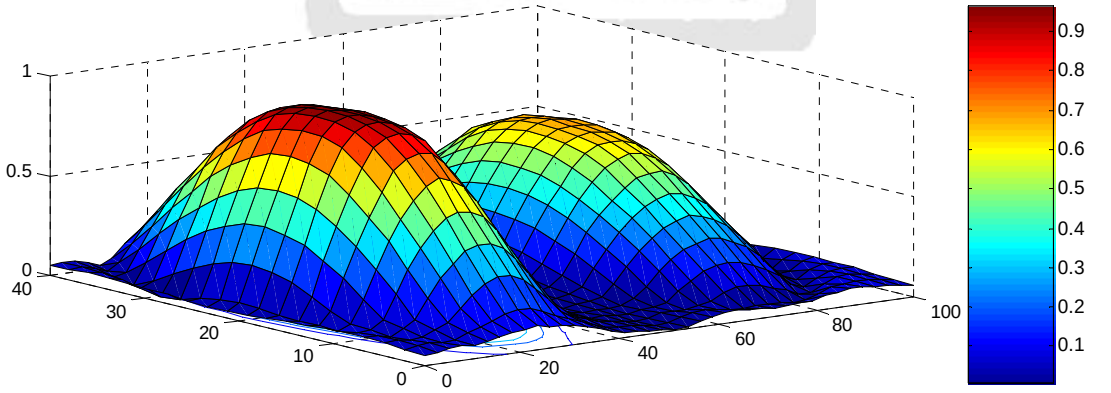

(b)

Figure 3.1. The magnitude of the magnetic field distributions around the coil in the TMS from (a) 2D-view and (b) 3D-view recorded at 50% of maximum power without shielding right the coil surface.

3.1.1. Effects in direction of flux magnetic field

Figure 3.2 shows the distribution of magnetic field in 3D distribution along the coil, The distribution of the resultant magnetic field of coil is obtained by adding up the magnetic intensity of each axis ($R = \sqrt{F_x^2 + F_y^2 + F_z^2}$). It is found that the distance along the z axis greatly influences the resultant distribution, while the influence of x and y axis is not significant. Consequently, the distributions of magnetic field of the following experiments are mainly conducted with shifting in z axis. The HPRs of the resultant flux magnetic field in perpendicular to XY plane flux magnetic field are shown in Figure 3.3.

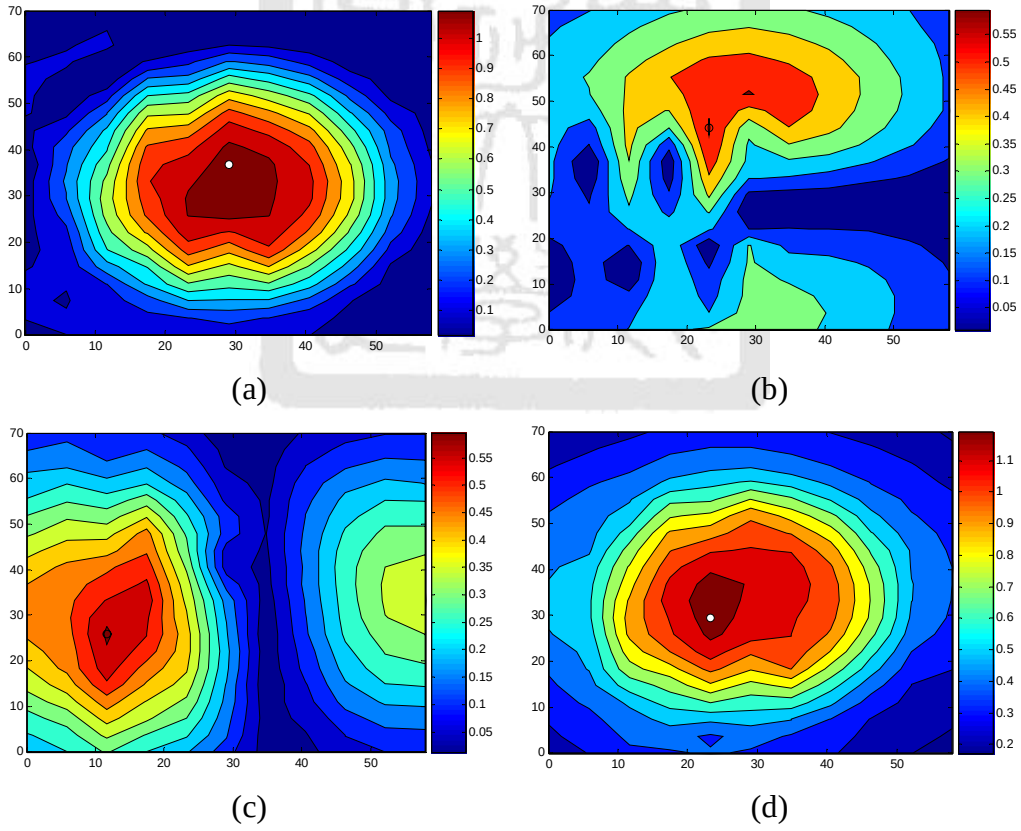

Figure 3.2. The distributions of the magnetic field of directions of (a) in perpendicular to XY plane, (b) in perpendicular to ZX plane, (c) in perpendicular to ZY plane, and (d) resultant sum.

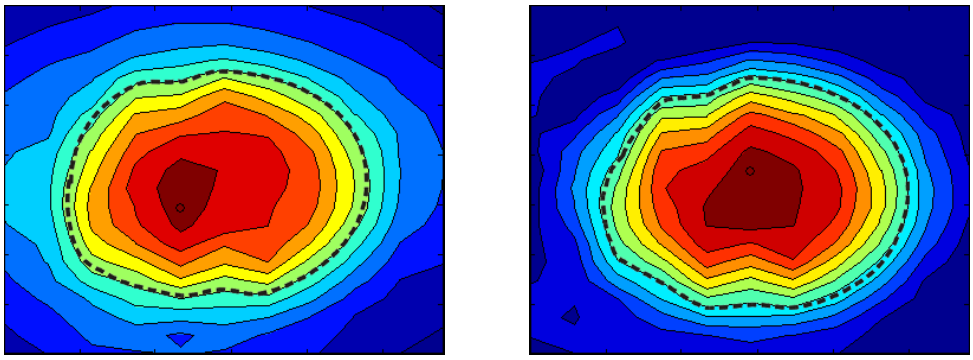

(a) resultant flux magnetic field (b) perpendicular to XY plane

Figure 3.3. The HPR of the magnetic field of (a) resultant flux magnetic field and (b) that in perpendicular to XY plane.

3.1.2. Effects of the power output

Figure 3.4 shows the distributions of magnetic field around the coil of different power outputs of TMS. The distributions of magnetic field were obtained is in proportional to the power output of rTMS. In these measurements, the position of origin point is defined at the lower left corner of coil. The peak magnetic filed of 0.190 T occurs at x=21.05 mm and y=21.05 mm with respect to the origin point at 10 % of power output. Similarly, peak intensity all occur at the close area with varied power outputs. The peak magnetic intensities were monotonic increase at 0.382 T, 0.590 T, 0.757 T, 0.971 T, 1.1880T with the increase of 20 % to 60 % of magnetic output of Rapid 2. We can observe that the distributions of magnetic field obtained is in proportional to the power output of the rTMS. The maximum magnetic field of 100% of output power is about 2 T. The linearity of the peak magnetic intensity to the power output of TMS is shown in Figure 3.5.

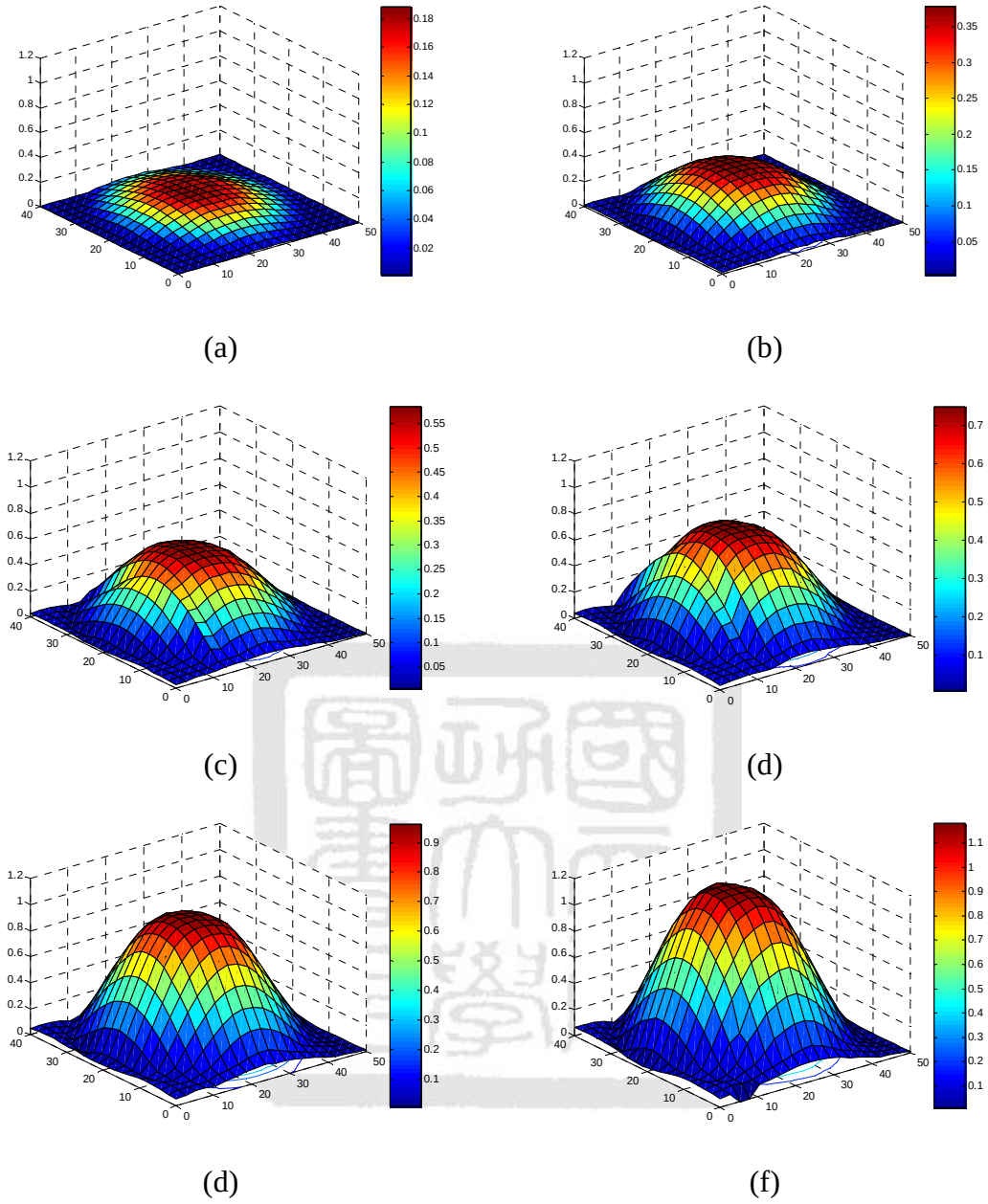

Figure 3.4. The distribution of magnetic field measured at power of (a) 10 %, (b) 20 %, (c) 30 %m (d) 40%m (d) 50 % and (e) 60 %.

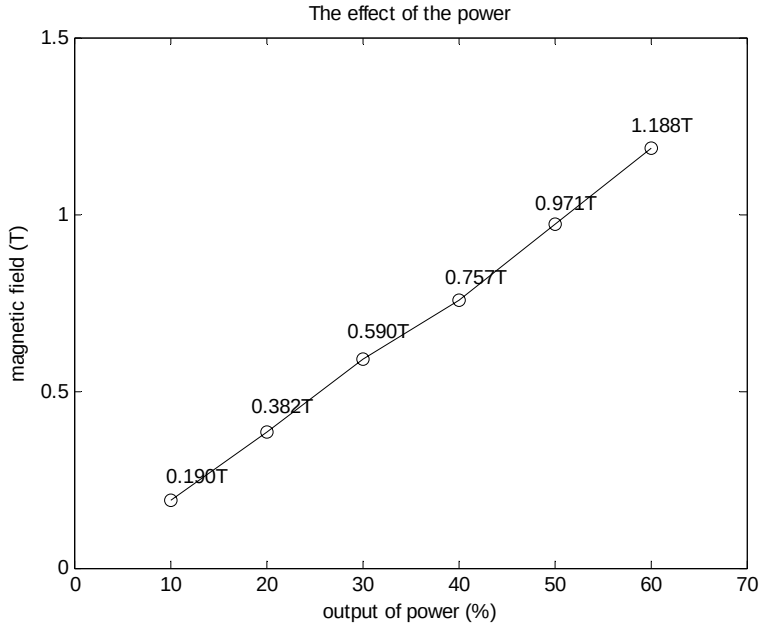

Figure 3.5. Measurements of the peak magnetic field with different TMS power outputs.

3.1.3. Effects of the distance

The distributions of the magnetic field under various distances between probe and coil surface with and without shielding are shown in Figure 3.6 and Figure 3.7. The power output was set at 50 %. The effect of the distance between the rTMS coil and the Hall probe, d, was observed along Z axis. The peak magnetic field measuring at d=2 mm is 0.841 T, which occurs at x=23.68 mm and y=23.16 mm. Similarly, the peak magnetic intensity are 0.731 T, 0.636 T, 0.496 T for measuring at a distance of 4 mm, 6 mm, and 8 mm, respectively. The peak intensities all occur at a very close area.

With the shielding of 3/4 of the corner, Figure 3.5 shows the peak magnetic field of 1.289 T occurring at x=21.05 mm and y=23.16 mm measured at d=2 mm. For other distances of 4 mm, 6 mm, and 8 mm, the peak occurs at the similar point but with a decreased peak intensity of 1.169 T, 0.805 T, and 0.615 T. The magnetic intensity decreases quickly with the increase of the depth. The linearity of the peak magnetic intensity to the different distances is shown in Figure 3.8.

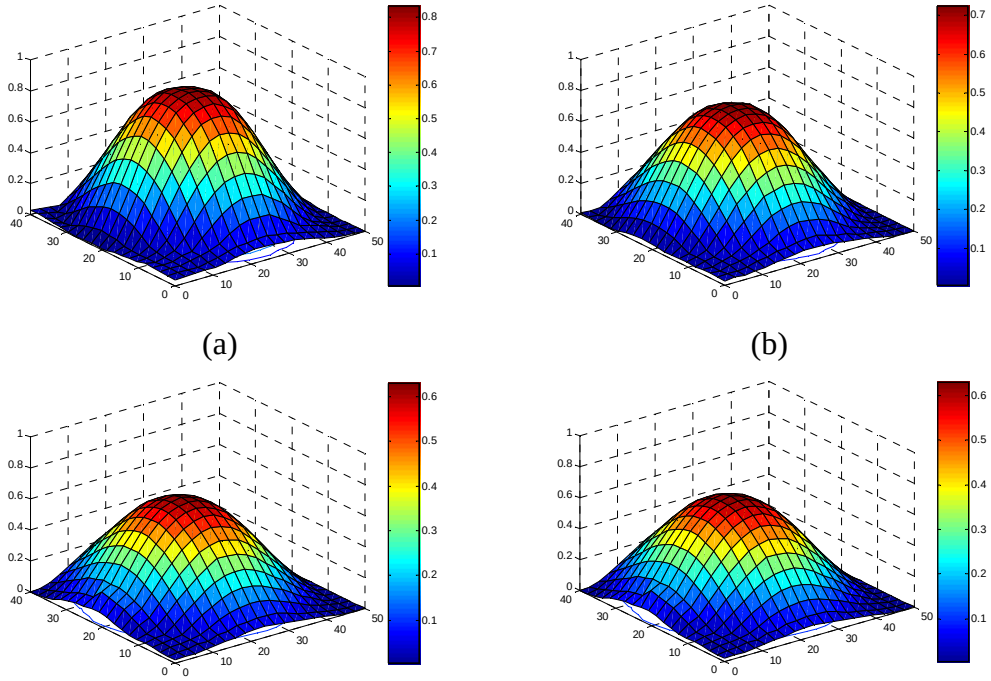

(a) (b)

(c) (d)

Figure 3.6. The distribution of the magnetic field with various distances of (a) 2 mm, (b) 4 mm, (c) 5 mm and (d) 8 mm to the surface of stimulation coil.

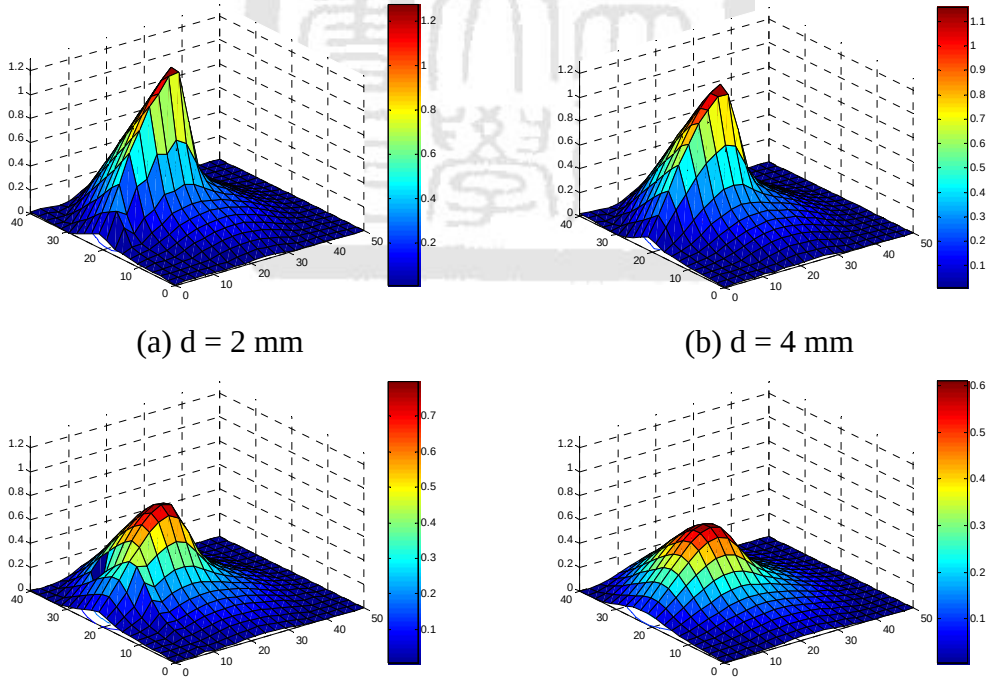

(a) d = 2 mm (b) d = 4 mm

(c) d = 6 mm (d) d = 8 mm

Figure 3.7. The distribution of the magnetic field under 3/4 of shielding plate with various distances of (a) 2 mm, (b) 4 mm, (c) 5 mm and (d) 8 mm to the surface of stimulation coil.

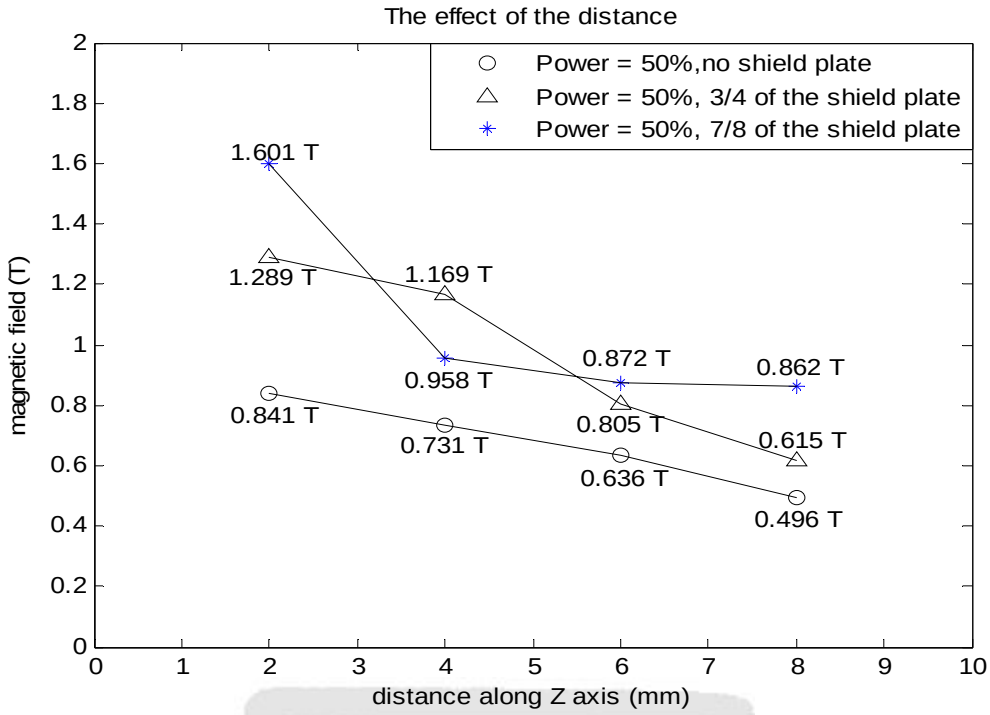

Figure 3.8. Measurements of magnetic fields at different distances.

3.1.4. Effects of the shielding plate and half power region

To compare the effects of the geometry form of the shield plate, Figure 3.9 shows the distribution of the magnetic field density masked by various shielding plates. Without the shielding plate, the peak magnetic field is about 0.841 T. With a hole at the center of shield plate, the peak magnetic field reduced significantly to 0.231 T occurring at a close position with that measured without shielding plate. The distribution of magnetic field was slightly distorted with shielding of half-size plate. However, the peak magnetic field was increased to 1.097 T. Similar observations can be found in one quarter, one eighth aperture and rectangular open area in the shielding plate. The magnetic field distribution was slightly distorted but an increase in the peak intensity of 1.289 T, 1.601 T and 1.275 T for these cases can be found.

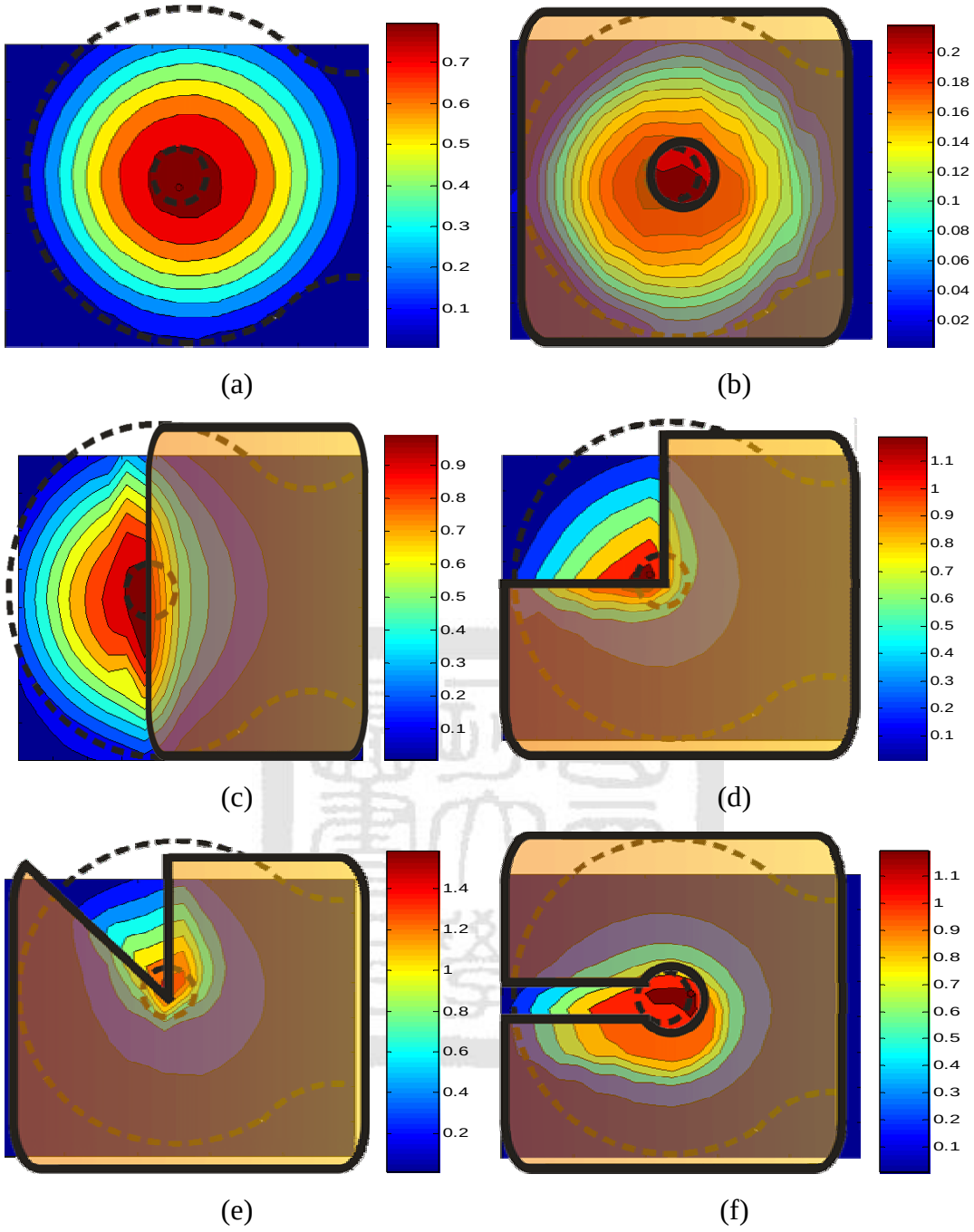

Figure 3.9. The distribution of the magnetic field for different shielding plates of (a) Without shield plate, (b) a hole on the center, (c) half-sized (d) a quarter window, (e) one eighth opening, and (f) opening rectangular window.

Figure 3.10 shows the area of HPRs generated by various shielding plates. Without the shielding plate, the area of HPR is about 726 mm^2 which accounts for 36.3% of total area. With a hole at the center of shield plate, the HPR area is about 603 mm^2 or 30.1% of total area. The HPR of magnetic field of half-size, one quarter, one eighth shielding were reduced to 433 mm^2, 205 mm^2, and 109 mm^2 or about 21.6%, 10.2 %, and 5.4 % of total area. Similar observations can be found in the rectangular opening in the shielding plate. Decreased HPR of 305 mm^2 or 15,2 % of total area can be found.

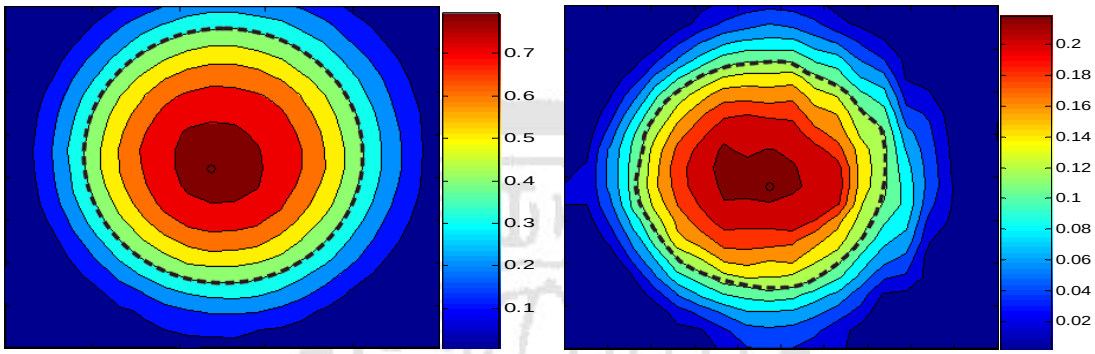

(a) (b)

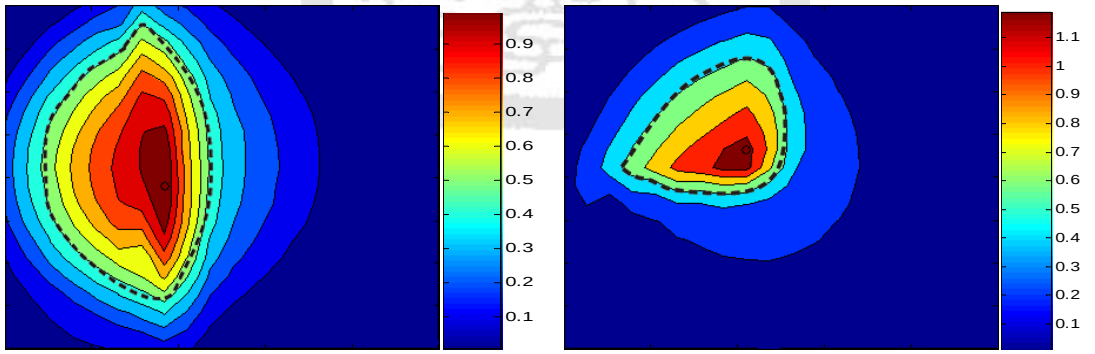

(c) (d)

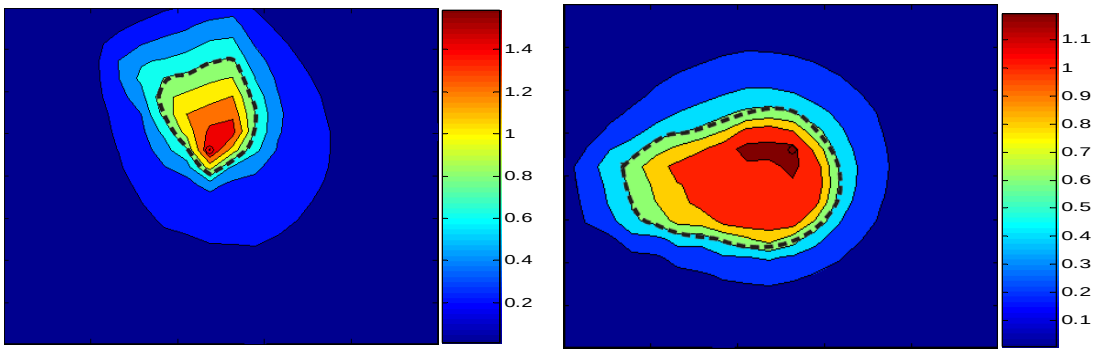

(e) (f)

Figure 3.10. The HPR of the magnetic field with different shielding plate of (a) without shielding, (b) a hole on the center , (c) half-sized shielding (d) a quarter of the shielding (e) one eighth of the shielding, and (f) open rectangular window of the shield plate.

3.2 Experimental setup for rTMS tested in small animal

During the TMS with shield, the shock wave will cause loud sound which could cause auditory startle reflex (ASR) response instead of MEP in rat. The occurrence of ASR could inhibit the occurrence of MEP. Thus, proper measures needed to reduce the sound generated during shielded TMS to obtain MEP. In order to reduce the sound, a buffer was inserted between coil and shield with holes to let out shock wave. Figure 3.11 shows an MEP induced without shielding and ASR elicited under half shielding condition. Compared with MEP of no shielding, the ASR potentials induced by half shielding exhibited longer onset latency, longer duration of evoked potential [23]. To determine the sound level for evoking ASR, digital sound level meter (JIN BOMB, LTD. TES – 1350A) was used for varied conditions. The distance between coil surface and microphone of sound meter on the normalized field along Z axis is shown in Figure 3.12. Figure 3.13 shows the sound level in decibel under different shielding plates. We can observe that more shielding will generate louder sound. The

sound level originated from TMS only was always below 96 dB. To determine the sound level causing ASR, TMS with shield was used for this purpose in which the magnetic field has been reduced below the MEP threshold. Then, a series of stimulation intensities from 10 % to 100 % was elicited to determine the threshold of sound level using a digital sound level meter for ASR. The experiment for rat-1 indicated that ASR was elicited above 110 dB at 100 % of TMS but the threshold for rat-2 is about 102 dB at a power output of 40% TMS. Figure 3.11 shows a MEP induced without shielding and ASR elicited under half shielding condition. Compare with no shielding MEP, the ASR potentials induced by half shielding was shown to have longer onset latency, longer duration of evoked potential [23].

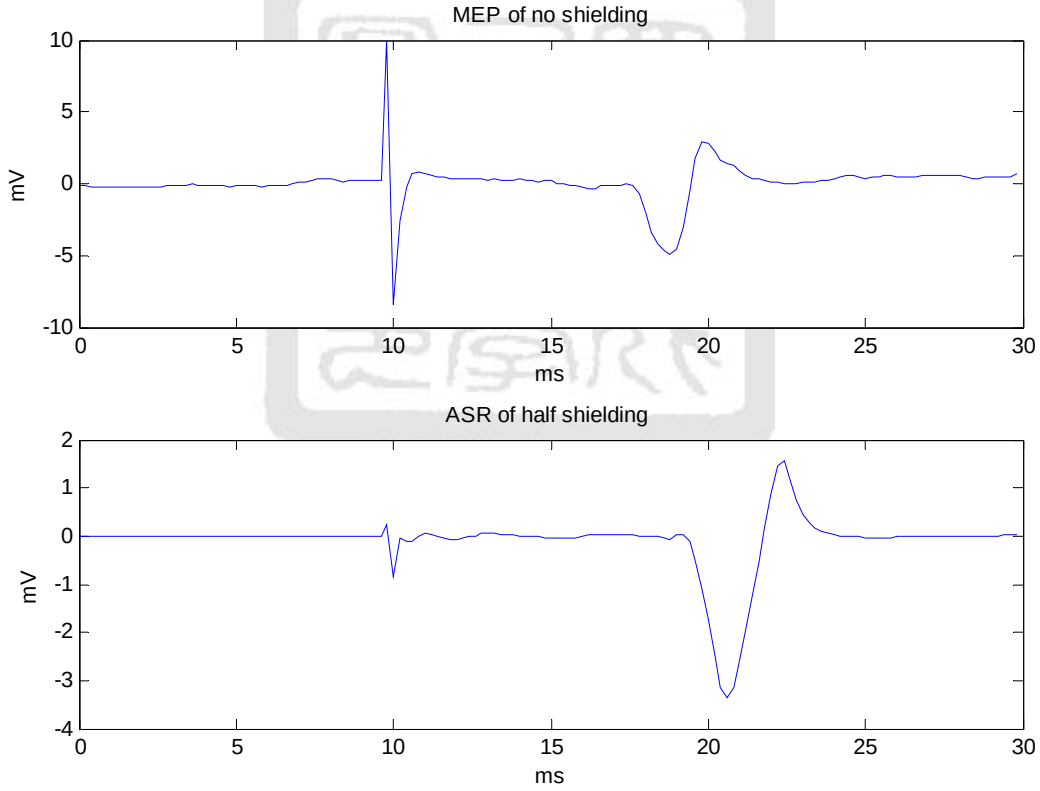

Figure 3.11. (a) MEP induced by magnetic stimulation and (b) ASR induced by sound during half shielding of magnetic stimulation.

Figure 3.12. The use of digital sound level meter to measure the sound level for determining the threshold for ASR.

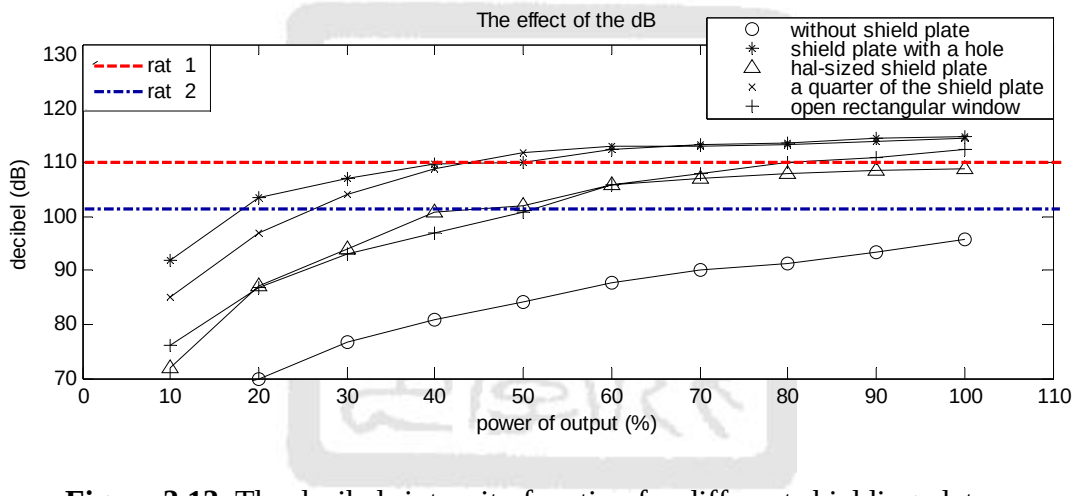

Figure 3.13. The decibel -intensity function for different shielding plates.

Figure 3.14 shows the MEP response with the increase of stimulation intensity which was recorded with the half-sized shielding plate in comparison with that without shielding. With the increase of stimulation intensity, the amplitude of MEP increased. The MT was about 54% power output under no shielding but increased to 70% with half-sized shielding plate. Similarly, the MT for rat-2 was 30% of TMS for no shielding and 40% for half-shielded TMS. At 120 % stimulation of the MT, the amplitude of MEP's in rat 1 was 2.0 mV for no shielding in comparison with 1.32 mV for half-sized shielding. At 120 % of MT, the MEP amplitude of rat-2 was 6.8 mV for no shielding but it reached 7.99 mV with half-sized shielding.

The MT of rat-1 was 40 % with half-sized shielding and the threshold for ASR was above 110dB. We can confirm under 140% of MT that the MEP of rat-1 was induced by magnetic field. In addition, the rat-2 was anaesthetized with different chloral which led to more sensitive to stimulation. The MT of rat-2 was 40 % with half-sized shielding and the ASR threshold was about 102 dB.

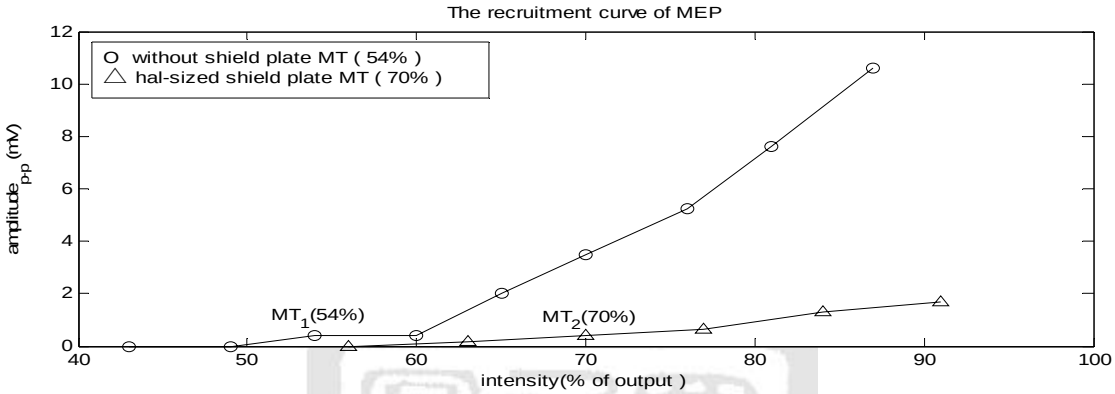

(a)

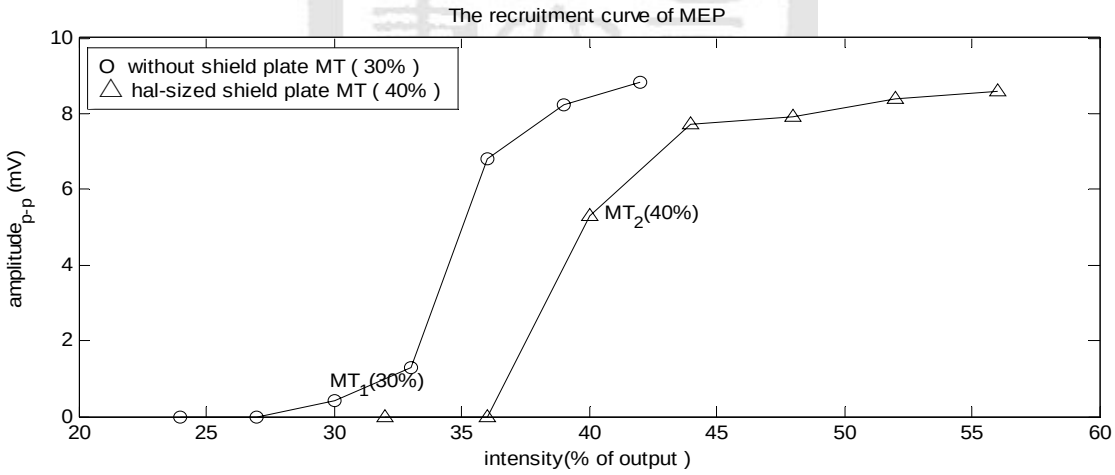

(b)

Figure 3.14. The amplitude-intensity curve for evoking MEP for (a) rat-1 and (b) rat-2.

Chapter 4 Discussion and Conclusion

A magnetic field distribution measurement platform was established in this study. The platform can be used to measure the magnetic field distribution of various experiment designs. First, the distribution of Magstim FOE coil was measured which is inconsistent with a common FOE coil in which symmetrical distribution should be presented. However, the distribution was miniature FOE is slightly asymmetrical which is due to the distance between the left coil and right coil too far away and leads to a peak magnetic flux at the coil center. Consequently, the distribution of Magstim FOE coil is similar to two independent circuit coils. We also validate that the magnetic intensity of z axis influences more on the overall distribution, while the influence of x and y axis is less significant.

We have designed various types of shielding plates for localized magnetic stimulation of the rat brain. This design can produce higher localization than the FOE coil and circuit coil. The important factors are the type of shielding plate and the opening of the shielding for localization. The choice of the shielding plate should be copper with more than 1 mm in thickness. A hole in the shielding would reduce the overall magnetic field which can not achieve the localization of magnetic stimulation. Opening in the shielding can provide localization stimulation. As the shielding area reduced, it is apparent that the magnetic field can be effectively focused under the opening window. The shielding with opening can prevent other parts of the brain from exposure to high magnetic fields. Under the same power output condition, the intensity of magnetic field with the shielding plate is higher than that without the shielding. This is because the shielding plate can guide the magnetic flux towards the opening and thus elevate the magnetic intensity in the area under the opening. However, our animal experiment indicating that a narrowed opening with a higher

magnetic intensity can not elicit MEP. From the Faraday law, the electrical field is proportional to the covering area. Thus, a smaller area of stimulation with high magnetic intensity might not induce sufficient electric field to elicit MEP.

$$V = -N\frac{d\phi}{dt} \quad \text{and} \quad \phi = \int_S B\ ds$$

where V is the induce electric field, B is the magnetic field produced by the coil, Φ is the magnetic flux and S is the area of the stimulation. Thus, a compromise between the localization and induced electrical field should be made in small animal study.

By applying the shielding could cause another side effect, ASR, a reflex evoked by loud sound from the shock wave again the shielding during magnetic stimulation. The ASRs in general are smaller, less reproducible, and with longer latencies than those of MEPs. Our experiments indicated that the ASR level might be varied in different animal. A sound level below 96 dB is suggested for not eliciting ASR. Another possibility is to incorporate sound proof chamber for the small animal that could avoid the occurrence of ASR for our MEP experiment.

In conclusion, our experiment indicated that shielding plate applied to the conventional FOE coil can lead to significant improvement in localization but the induced electric field has been reduced and a loud sound can cause interference from ASR. Thus, optimization between these three factors, reduced stimulation area, increased electrical field, and a louder sound for ASR interference should be made for TMS assessment of motor excitability as well as for rTMS treatment in small animal experiment.

References

[1] M. S. George, "Stimulating the brain," *Sci Am,* vol. 289, pp. 66-73, Sep 2003.

[2] K. M. Rosler, "Transcranial magnetic brain stimulation: a tool to investigate central motor pathways," *News Physiol Sci,* vol. 16, pp. 297-302, Dec 2001.

[3] A. A. Gershon, P. N. Dannon, and L. Grunhaus, "Transcranial magnetic stimulation in the treatment of depression," *Am J Psychiatry,* vol. 160, pp. 835-845, May 2003.

[4] V. W. Lin, I. N. Hsiao, and V. Dhaka, "Magnetic coil design considerations for functional magnetic stimulation," *IEEE Trans Biomed Eng,* vol. 47, pp. 600-610, May 2000.

[5] K. H. Hsu and D. M. Durand, "A 3-D differential coil design for localized magnetic stimulation," *IEEE Trans Biomed Eng,* vol. 48, pp. 1162-1168, Oct 2001.

[6] C. Ren, P. P. Tarjan, and D. B. Popovic, "A novel electric design for electromagnetic stimulation--the Slinky coil," *IEEE Trans Biomed Eng,* vol. 42, pp. 918-925, Sep 1995.

[7] K. Davey and C. M. Epstein, "Magnetic stimulation coil and circuit design," *IEEE Trans Biomed Eng,* vol. 47, pp. 1493-14939, Nov 2000.

[8] S. Luquet, V. Barra, and J. J. Lemaire, "Transcranial Magnetic Stimulation : Magnetic Field Computation in empty free space," *Conf Proc IEEE Eng Med Biol Soc,* vol. 4, pp. 4365-4368, 2005.

[9] C. M. Epstein and K. R. Davey, "Iron-core coils for transcranial magnetic stimulation," *J Clin Neurophysiol,* vol. 19, pp. 376-381, Aug 2002.

[10] B. H. Han, I. K. Chun, S. C. Lee, and S. Y. Lee, "Multichannel magnetic stimulation system design considering mutual couplings among the

stimulation coils," *IEEE Trans Biomed Eng,* vol. 51, pp. 812-817, May 2004.

[11] D. H. Kim, G. E. Georghiou, and C. Won, "Improved field localization in transcranial magnetic stimulation of the brain with the utilization of a conductive shield plate in the stimulator," *IEEE Trans Biomed Eng,* vol. 53, pp. 720-725, Apr 2006.

[12] K. R. Davey and M. Riehl, "Suppressing the surface field during transcranial magnetic stimulation," *IEEE Trans Biomed Eng,* vol. 53, pp. 190-194, Feb 2006.

[13] T. R. Han, J. H. Kim, and J. Y. Lim, "Optimization of facilitation related to threshold in transcranial magnetic stimulation," *Clin Neurophysiol,* vol. 112, pp. 593-599, Apr 2001.

[14] J. Ruohonen, P. Ravazzani, F. Grandori, and R. J. Ilmoniemi, "Theory of multichannel magnetic stimulation: toward functional neuromuscular rehabilitation," *IEEE Trans Biomed Eng,* vol. 46, pp. 646-651, Jun 1999.

[15] J. Zheng, L. Li, and X. Huo, "Analysis of Electric Field in Real Rat Head Model during Transcranial Magnetic Stimulation," *Conf Proc IEEE Eng Med Biol Soc,* vol. 2, pp. 1529-1532, 2005.

[16] J. Sommer, A. Jansen, B. Drager, O. Steinstrater, C. Breitenstein, M. Deppe, and S. Knecht, "Transcranial magnetic stimulation--a sandwich coil design for a better sham," *Clin Neurophysiol,* vol. 117, pp. 440-446, Feb 2006.

[17] S. Yang, G. Xu, L. Wang, Y. Chen, H. Wu, Y. Li, and Q. Yang, "3D realistic head model simulation based on transcranial magnetic stimulation," *Conf Proc IEEE Eng Med Biol Soc,* vol. Suppl, pp. 6469-6472, 2006.

[18] D. Liebetanz, S. Fauser, T. Michaelis, B. Czeh, T. Watanabe, W. Paulus, J. Frahm, and E. Fuchs, "Safety aspects of chronic low-frequency transcranial magnetic stimulation based on localized proton magnetic resonance

spectroscopy and histology of the rat brain," *J Psychiatr Res,* vol. 37, pp. 277-286, Jul-Aug 2003.

[19] A. Thielscher and T. Kammer, "Electric field properties of two commercial figure-8 coils in TMS: calculation of focality and efficiency," *Clin Neurophysiol,* vol. 115, pp. 1697-1708, Jul 2004.

[20] G. Xu, Y. Chen, S. Yang, M. Wang, and W. Yan, "The optimal design of magnetic coil in transcranial magnetic stimulation," *Conf Proc IEEE Eng Med Biol Soc,* vol. 6, pp. 6221-6224, 2005.

[21] R. C. de Sauvage, I. Lagroye, B. Billaudel, and B. Veyret, "Evaluation of the potential genotoxic effects of rTMS on the rat brain and current density mapping," *Clin Neurophysiol,* vol. 119, pp. 482-491, Feb 2008.

[22] A. R. Luft, A. Kaelin-Lang, T. K. Hauser, L. G. Cohen, N. V. Thakor, and D. F. Hanley, "Transcranial magnetic stimulation in the rat," *Exp Brain Res,* vol. 140, pp. 112-121, Sep 2001.

[23] R. D. Linden, Y. P. Zhang, D. A. Burke, M. A. Hunt, J. E. Harpring, and C. B. Shields, "Magnetic motor evoked potential monitoring in the rat," *J Neurosurg,* vol. 91, pp. 205-210, Oct 1999.